Supporting Information for Publication

Characterising Nanoparticles in Biological Matrices: Tipping Points in Agglomeration State and Cellular Delivery *In Vitro*

John W. Wills, Huw D. Summers, Nicole Hondow, Aishwarya Sooresh, Kenith E. Meissner, Paul A. White, Paul Rees, Andy Brown, Shareen H. Doak.

List of supporting information –

Table S1 – Summary of stock nanoparticle physico-chemical characterisation data.

Figure S1 – Supporting physico-chemical characterisation data collected by transmission electron microscopy and energy dispersive X-ray (EDX) spectrometry.

Figure S2 – 3-D "Z-stack" reconstruction of optical sections obtained by confocal microscopy. This shows that the polystyrene-latex (PS) nanoparticles were internalised by the TK6 cells.

Figure S3 – PS nanoparticle fluorimetry results. These show nanoparticle fluorescence was extremely stable under experimentally-relevant conditions and thus could be used reliably to measure cellular dose.

Figure S4 – PS nanoparticle cell viability analysis. These confirm that the PS nanoparticles had no impact on TK6 cell viability.

Figure S5 – Further confocal micrographs supporting the imaging cytometry study. These provide further examples of PS nanoparticle cellular delivery across dose and serum environment combinations.

Figure S6 – Agglomeration state analysis by cryogenic snapshot sampling (CSS) and transmission electron microscopy (TEM). This figure presents a schematic overview of the image analysis method used for agglomeration state determination by the CSS-TEM approach.

Video S1 – Typical "tilt-series" image sequence showing the 3-D reconstruction of a nanoparticle agglomerate. This approach allowed the 3-D morphology of CSS sampled agglomerates to be measured.

Figure S7 – Assessing agglomerate 3-D morphology using tilt-series image sequences. These data permitted empirical validation of the scaling model used to estimate agglomerate volume from the 2-D CSS-TEM images.

Figure S8 – Fluorimetry studies. These show the fluorescence emission of the PS nanoparticles is a function of nanoparticle volume.

Table S2 – Alternative dose metrics for the PS and silicon dioxide (SiO_2) nanoparticle exposures used in this study.

Figure S9 – "Benchmark dose" dose-response modeling results. These scrutinise the effect of serum environment on SiO_2 nanoparticle toxicity.

Figure S10 – S13 Further sectioned-cell electron micrographs showing differences in the cellular delivery of the SiO_2 nanoparticles across the different serum environments.

Figure S14 – Graphic showing the relationship between the total surface areas of the administered doses alongside the presence or absence of "tipping points" in the nanoparticles' agglomeration state.

Table S1 – Supporting nanoparticle physico-chemical characterisation data: TEM in conjunction with energy dispersive X-ray (EDX) spectroscopy was used to determine primary size distributions, shape / morphology, crystallinity, composition and purity. Dynamic light scattering (DLS) was used to determine colloid stability / agglomeration state (hydrodynamic diameter) and also nanoparticle surface charge (zeta potential) in as-manufactured aqueous solution.

			Transmission Electron Microscopy / Energy Dispersive X-ray Spectroscopy					**Dynamic Light Scattering:** Peak analysis of distributions by particle number				
Product Name (stock solution type)	**Text Reference**	**Manufacturer Specified Size:** diameter, nm	**Primary Size:** average diameter, nm ± standard deviation (range)	**Shape / Morphology**	**Crystallinity / Composition & Purity** Contaminant free?	**Material Density:** g/cm^3	**Material Refractive Index**	**Agglomeration:** hydrodynamic diameter, nm			**Surface Charge:** mV	**Surface chemistry**
								aqueous dispersions				
								Modal size: distribution peak max (solution concentration)	Size Range: 99% number distribution	Polydispersity Index: range	Zeta Potential: mV ±SD *(Solution pH)*	
carboxylated 20 nm FluoSphere® (aqueous solution)	20 nm-PS	20	23.2 ±4.8 (13 – 35)	spherical/ smooth	amorphous polystyrene-latex, yes	1.05	1.58	24 (50 nM)	18 – 50	0.1 – 0.2	-63.2 ±4.1 *(pH 5.2)*	negative due to dissociated surface carboxyl groups
carboxylated 40 nm FluoSphere® (aqueous solution)	40 nm-PS	40	40.8 ±7.3 (24 – 60)	spherical/ smooth	amorphous polystyrene-latex, yes	1.05	1.58	55 (20 nM)	28 - 100	0.1 – 0.2	-50.4 ±8.3 *(pH 4.5)*	
Levasil® 200 (aqueous solution)	16nm-SiO_2	15	16.4 ± 5.3 (8 – 42)	spherical/ smooth	amorphous SiO_2, yes	2.65	1.54	17 (73 nM)	9 - 32	0.02 - 0.08	-63.1 ±3.84 *(pH 7.8)*	negative due to unbound surface oxygen
Levasil® 50 (aqueous solution)	85nm-SiO_2	55	85.1 ± 23.7 (41 – 159)	spherical/ smooth	amorphous SiO_2, yes	2.65	1.54	92 (0.5 nM)	50 - 164	0.21 - 0.22	-55.3 ±2.29 *(pH 9.4)*	

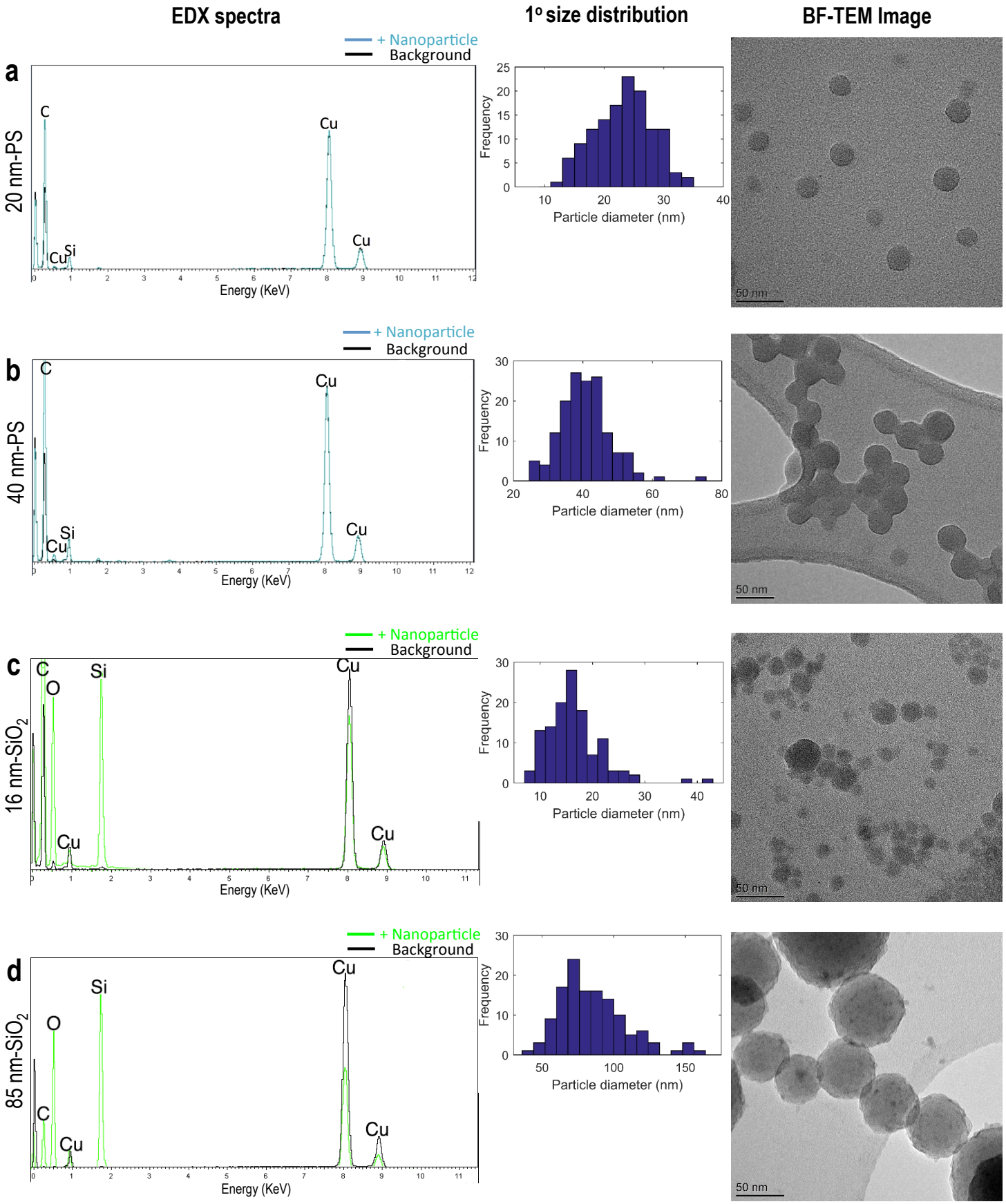

Figure S1 – Size, shape/morphology, crystalinity, composition and purity physico-chemical characterisation by transmission electron microscopy (TEM) and energy dispersive X-ray (EDX) spectrometry: (Left) (**a/b**) EDX analysis showed shifts in the ratio of carbon and (**c/d**) silicon and oxygen, confirming polystyrene latex and silicon dioxide nanoparticle compositions, respectively. No traces of particle / suspension-phase contaminants were found (Cu signal arose from use of copper sample grids). (Middle) 1º size distributions (i.e. individual particle measurements) for each nanoparticle type constructed from measurement of >100 nanoparticles / sample. (Right) Typical bright-field TEM micrographs from samples prepared by drop-casting aqueous solutions permitted visualisation of nanoparticle shape and morphology. No evidence of regular lattice planes was observed confirming all nanoparticles had amorphous chemical structures.

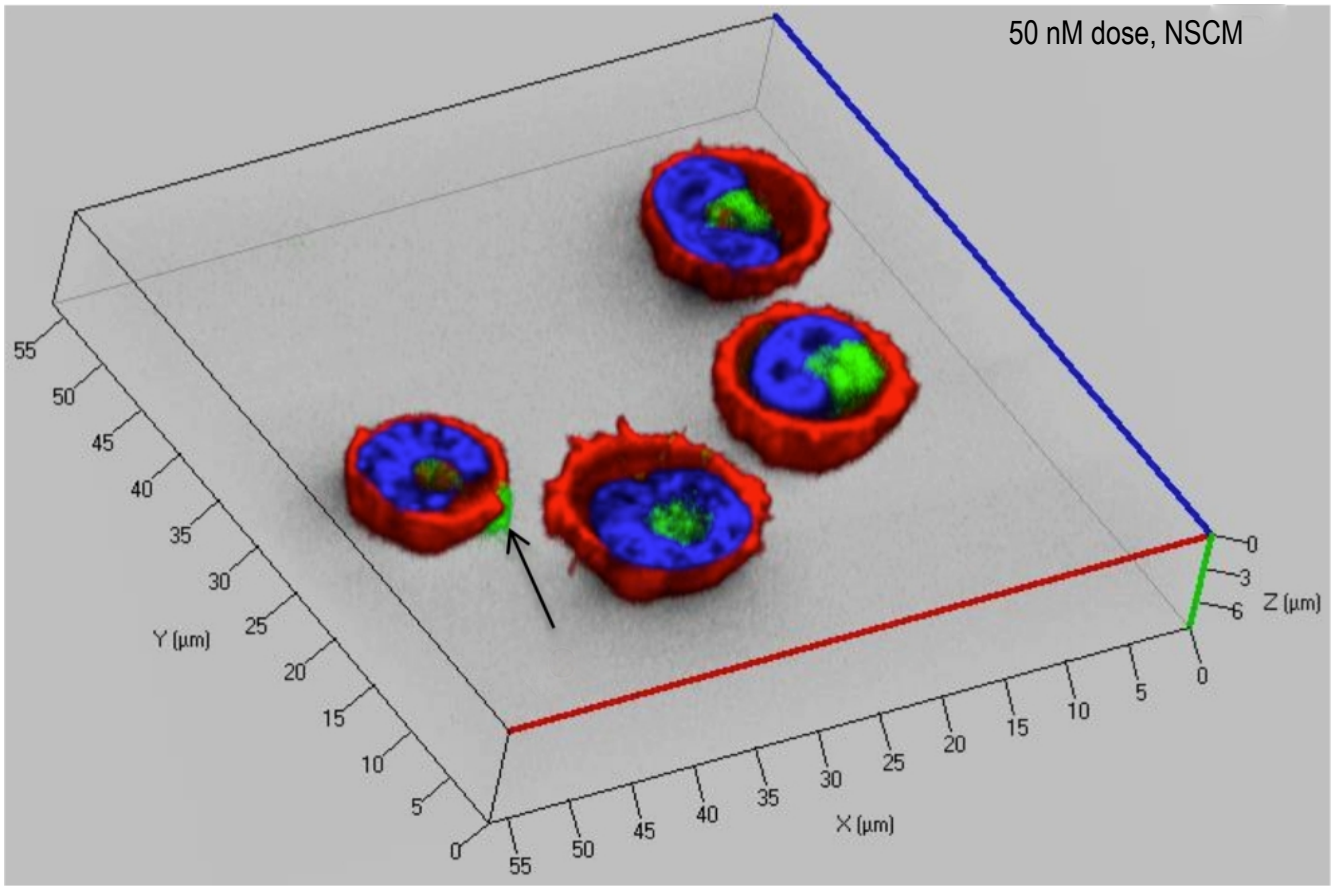

Figure S2 – 3-D reconstruction of confocal optical sections showing cellular internalisation of 20 nm-PS (24h exposure). Nanoparticles were internalised to the cytoplasm of the human B lymphoblast cells (TK6) (red = phalloidin-labeled cytoskeleton, green = nanoparticles, blue = Hoechst 33342-labeled nuclei). Changes in agglomerate size influenced the proportion of the dose internalised versus bound to the cell surface (e.g. larger, cell-membrane bound agglomerate indicated by arrow).

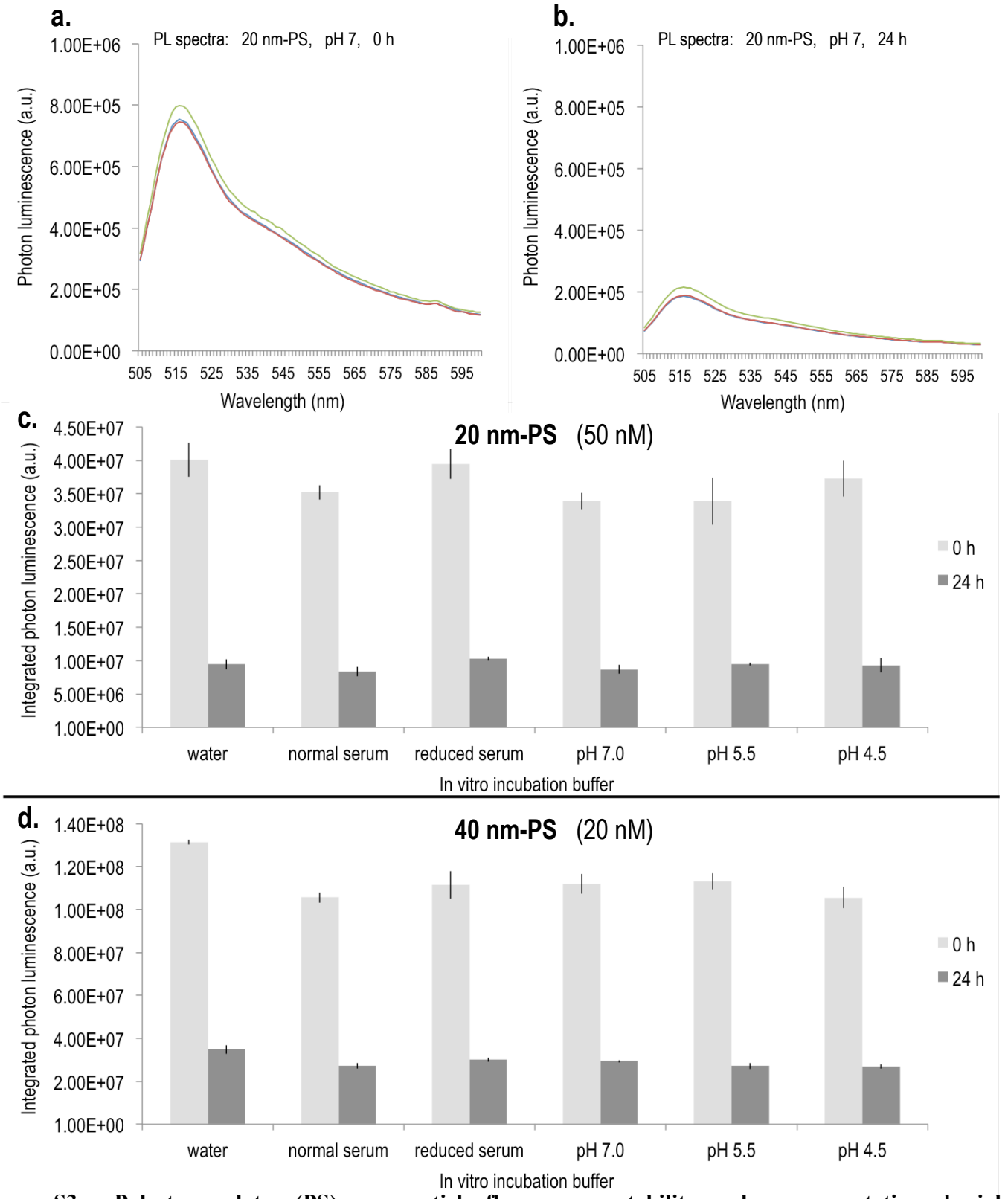

Figure S3 – Polystyrene-latex (PS) nanoparticle fluorescence stability under representative physiological conditions. PS nanoparticle photon luminescence (i.e. fluorescence emission) was measured by spectrofluorimetry at 0 h (representative spectra (n = 3) from the pH 7-buffered incubation shown, **a**) and after 24 h incubation (representative spectra (n = 3) from the pH 7-buffered incubation shown, **b**) in water, normal and reduced serum containing media, as well as in three buffers of differing pH that were designed to mimic different stages of the endosomal-lysosomal life-cycle[57]. Regardless of environment, 20 nm-PS (**c**) and 40 nm-PS (**d**) photon luminescence remained highly similar after 24 h incubation showing that PS nanoparticle fluorescence could reliably be used to determine cellular dose (n = 3, error bars = SD). Fluorescence stability was assessed by integration across the spectral emission range collected during the delivered-dose studies by imaging cytometry (i.e. 505 – 600 nm).

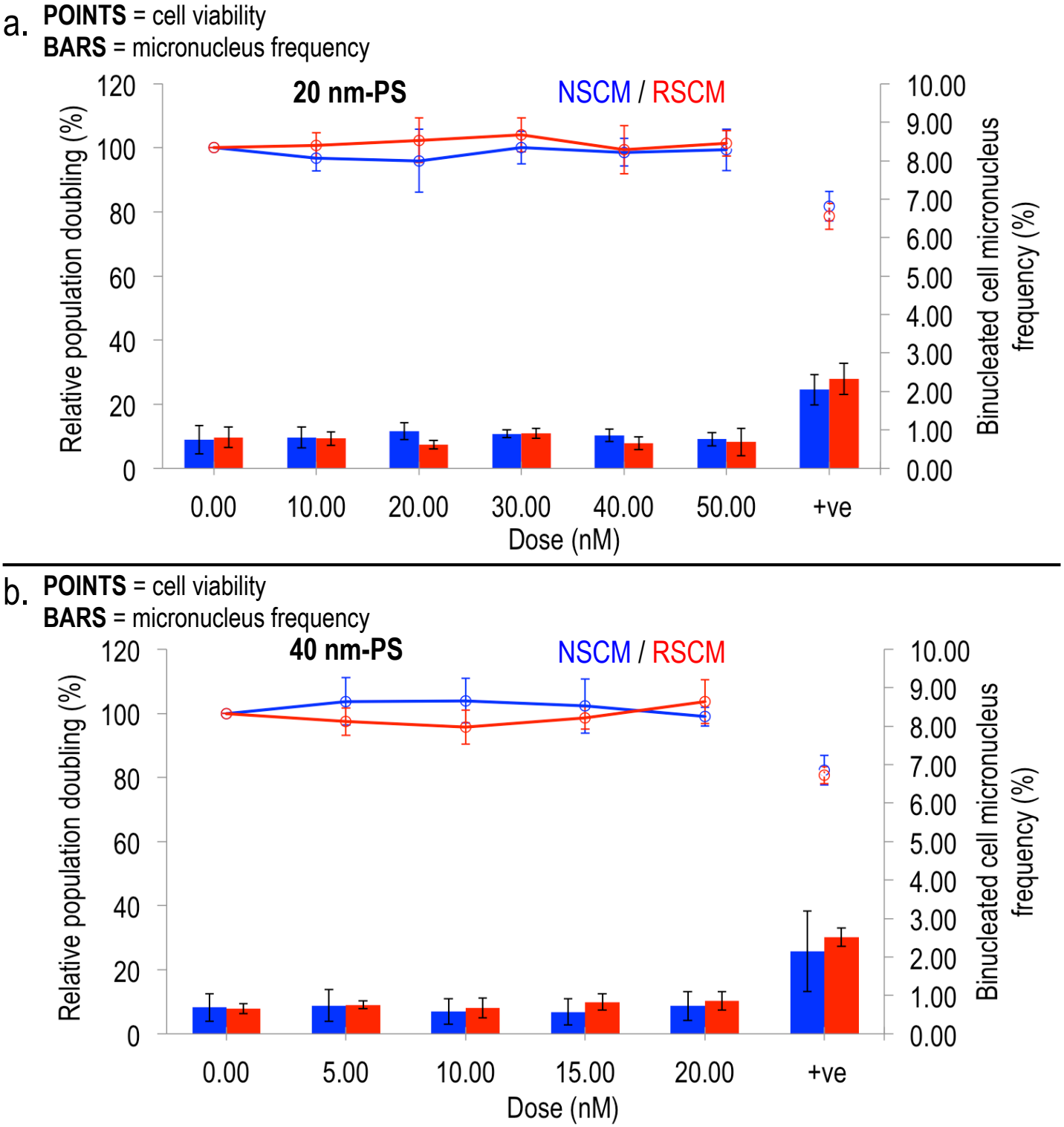

Figure S4 – Polystyrene-latex (PS) nanoparticle impact on TK6 cell viability. The effect of 24 h exposure to doses of 20 nm-PS (**a**) and 40 nm-PS (**b**) in terms of cell viability and DNA damage was assessed by relative population doubling (points) and the cytokinesis-blocked micronucleus assay (bars) (n = 3, error bars = SD, '+ve' = positive control). No adverse response was detected in either normal (NSCM) or reduced (RSCM) serum containing growth medium, for either endpoint, to the maximum tested nanoparticle concentrations used herein (≤ 50 nM). The PS nanoparticles thus comprised an excellent model for studying nanoparticle / agglomerate cellular delivery – as cells were not "lost" from the analysis due to cytotoxicity.

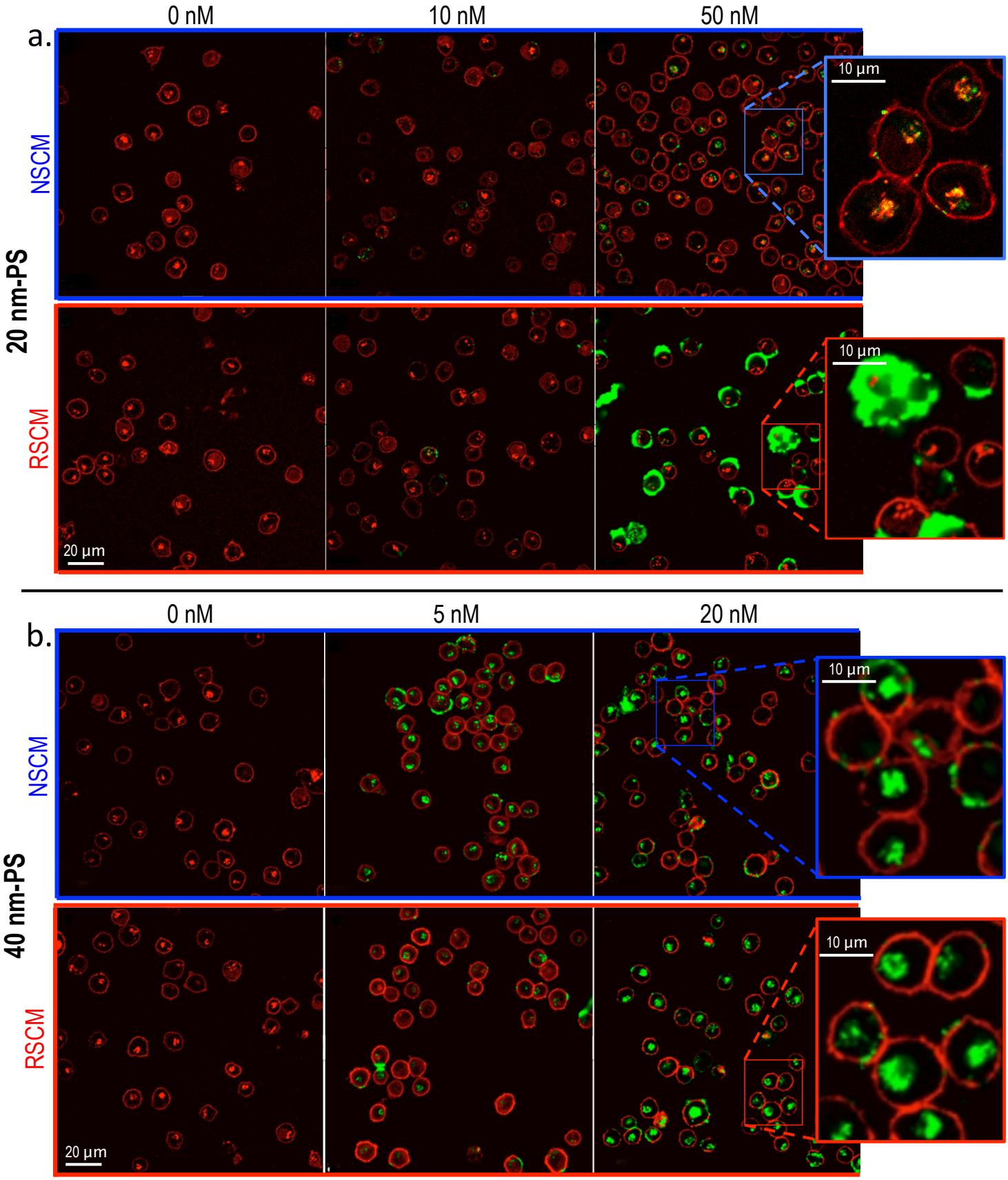

Figure S5 – The cellular delivery of polystyrene-latex (PS) nanoparticles after 24 h exposure *in vitro*. a/b Further confocal micrographs supporting the imaging cytometry study. **a**, The delivered cellular dose of 20 nm-PS administered at 10 nM concentration was highly similar in normal (NSCM) and reduced (RSCM) serum containing growth media. In contrast, it increased dramatically in RSCM alone when the nanoparticle dose was administered at 50 nM concentration. Meanwhile, (**b**) the delivered dose of 40 nm-PS remained highly similar in both serum environments regardless of dose. (Green = nanoparticles, red = wheat germ agglutinin-labeled cell membranes). Inset top right – the internalised nanoparticle signal typically colocalised (yellow) with signal from the membrane marker, indicative of particles taken-up in vesicles by endocytosis.

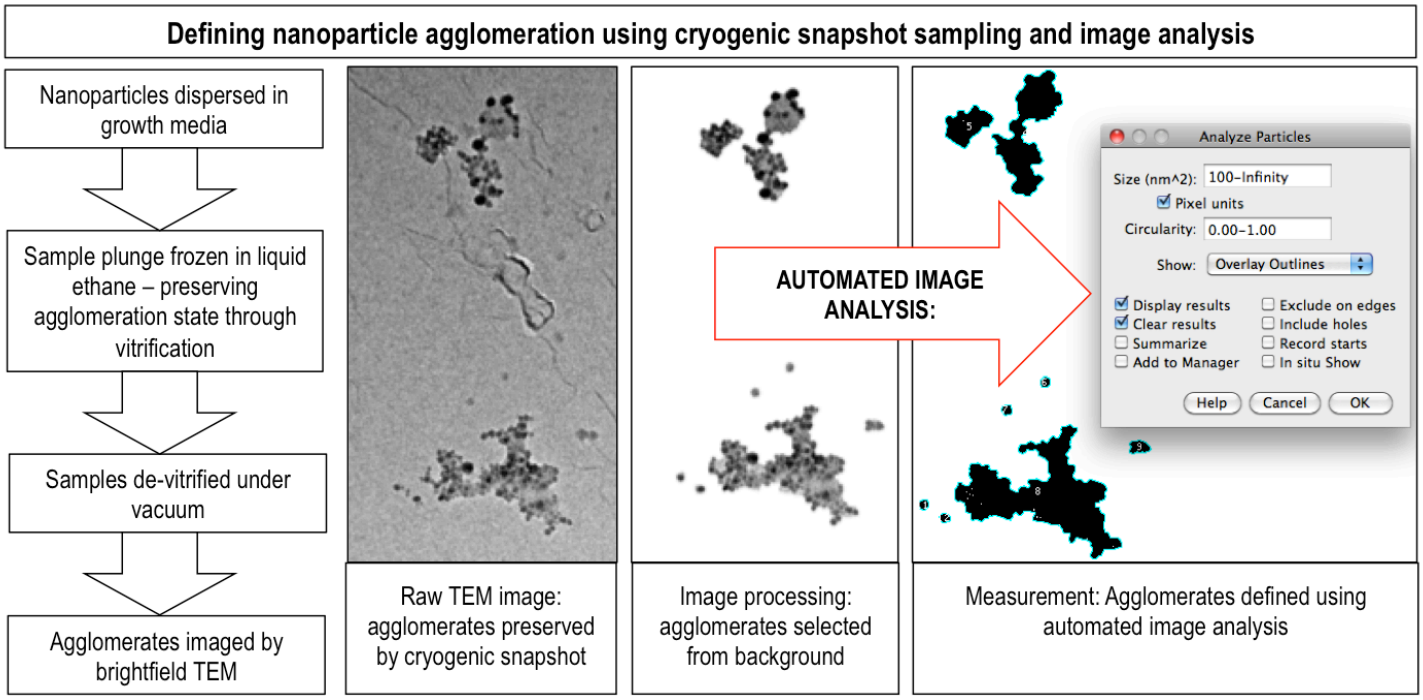

Figure S6 – The process of analysing nanoparticle agglomeration by cryogenic snapshot sampling, transmission electron microscopy and image analysis (CSS-TEM). a, Samples of nanoparticles dispersed in growth medium were prepared by plunge-freezing into liquid ethane, causing vitrification and accurate preservation of agglomeration states. These samples were then thawed under vacuum, facilitating sublimation of the aqueous phase, but leaving the agglomerates undisturbed and ready for imaging by conventional, bright-field transmission electron microscopy[20]. Individual nanoparticles / agglomerates in the collected raw electron micrographs (**b**) where manually segmented by tracing the outline of each agglomerate to remove the background (**c**) prior to automated image analysis using ImageJ (**d**). This approach permitted description of each agglomerate (~1,300 – 5,000 agglomerates analysed per dose / serum combination) according to any desired geometric parameter (*e.g.* Feret diameter, area, aspect ratio, circularity, perimeter, *etc.)*.

Supplementary Video S1 – Tilt-series image sequence of nanoparticle agglomerate ‘c’ (Supplementary Fig. 7; dimensions ~2.4 μm x ~1.3 μm x 250 ±50 nm) comprising 101 electron micrographs collected at 1 degree increments from +52° to -48°. This approach revealed the 3-D morphology of agglomerates collected by cryogenic snapshot sampling and permitted volume determination (i.e. the product of cross-sectional area and estimated z-thickness).

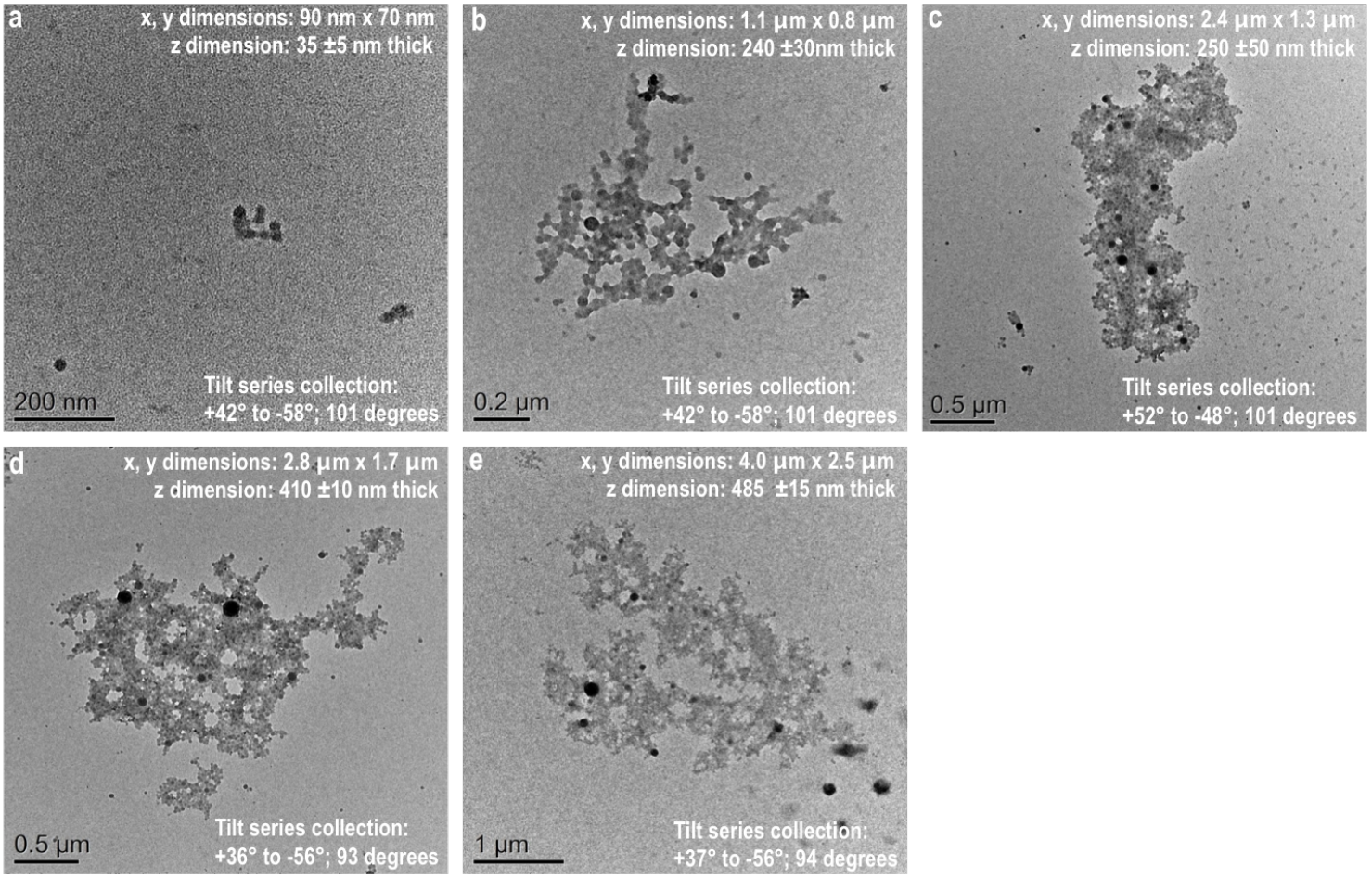

Figure S7 – Estimating agglomerate 3-D morphology. (**a-e**)**,** The area and volume of five cryogenic snap-shot sampled (CSS) agglomerates of varying size (~ 0.1, 1, 2, 3, 4 µm in diameter) was measured by 3-D reconstruction of electron micrographs obtained by rotating agglomerate specimens within the TEM and acquiring tilt-series datasets (93 – 101 images collected per agglomerate at 1 degree intervals; zero tilt shown) (see Supplementary Video S1 for example of tilt-series reconstruction and demonstration of single-particle resolution). These measured data were used to empirically validate the scaling model (i.e. volume = agglomerate area ^ scaling factor) used to transform the 2-D CSS-TEM agglomerate area data into estimated agglomerate volume.

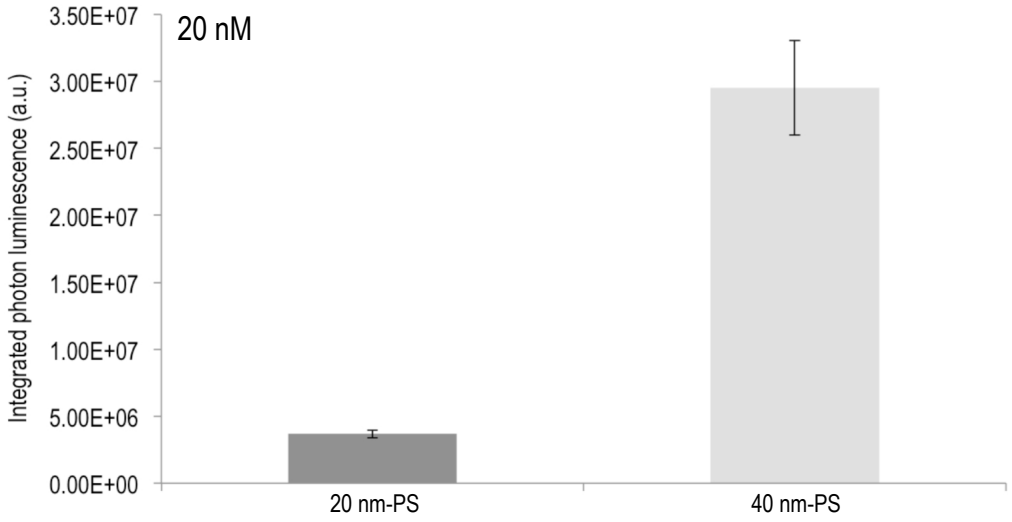

Figure S8 – Polystyrene-latex (PS) nanoparticle fluorescence intensity is a function of particle volume. The 20 nm-PS and 40 nm-PS used throughout this study were identical in all aspects except diameter. At equal number concentrations (20 nM), the photon luminescence (i.e. fluorescence emission) of the 40 nm particles was determined ~8.01 times brighter than the 20 nm particles across the spectral emission range collected during the imaging cytometry study (i.e. 505 – 600 nm) (n = 12; error bars = SD). This confirms PS fluorescence is a function of particle volume, as the volume of a 40 nm sphere is 8 times that of a 20 nm sphere.

Supplementary Table S2 – Alternative dose metrics. Below, the administered doses of polystyrene-latex (PS) and silicon dioxide (SiO_2) nanoparticles are provided in mass/volume and total surface area (nm^2) units to supplement the number/volume (i.e. nM) metric used throughout the manuscript.

Equivalent dose metrics:											
20 nm-PS			40 nm-PS			16 nm-SiO_2			85 nm-SiO_2		
nM	µg/mL	nm^2	nM	µg/mL	nm^2	nM	µg/mL	nm^2	nM	µg/mL	nm^2
0.0	0.0	0.00E+00	0.0	0.0	0.00E+00	0.0	0.0	0.00E+00	0.0000	0.0	0.00E+00
10.0	26.4	1.02E+17	5.0	105.9	1.57E+17	14.6	50.0	7.48E+16	0.0097	50.0	1.33E+15
20.0	52.8	2.04E+17	10.0	211.9	3.14E+17	29.2	100.0	1.50E+17	0.1947	100.0	2.67E+16
30.0	79.2	3.06E+17	15.0	317.8	4.72E+17	43.8	150.0	2.24E+17	0.2921	150.0	4.00E+16
40.0	105.6	4.08E+17	20.0	423.8	6.29E+17	58.4	200.0	2.99E+17	0.3894	200.0	5.33E+16
50.0	132.0	5.10E+17				73.0	250.0	3.74E+17	0.4868	250.0	6.66E+16
						87.7	300.0	4.49E+17	0.5842	300.0	8.00E+16

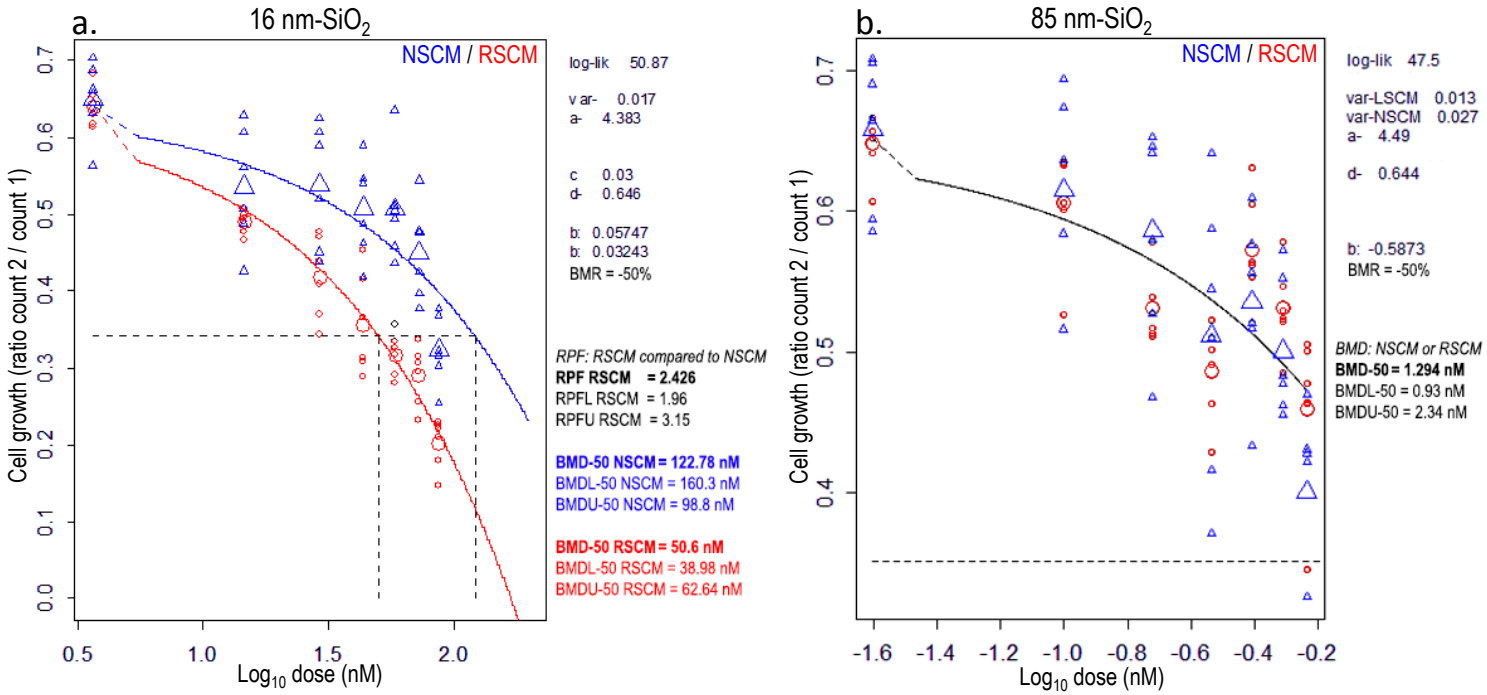

Figure S9 – Benchmark dose (BMD) modeling to determine the effect of serum environment on silica nanoparticle cytotoxicity. In each plot, the curves represent the fitted four-parameter exponential model to the dose-response data (where model parameter '*a*' = background response; '*b*' = potency; '*c*' = maximum response; '*d*' = log-steepness and '*var*' = within-group variation)[66]. (**a**) For the 16 nm-SiO_2 data, serum environment (NSCM = normal (10%) serum, RSCM = reduced (2%) serum) was determined as an influential covariate on the dose-response relationship. Thus, two curves are required to describe the cell-viability data: one for the NSCM datapoints and one in RSCM datapoints, respectively. (**b**) Contrastingly, *all* of the 85 nm-SiO_2 dose-response data (i.e. regardless of whether exposures were carried out in NSCM or RSCM) were found to be adequately described by a single curve (i.e. there was no serum-dependent effect). In turn, the BMD-50 values represent the best estimate of the dose that will elicit the pre-chosen benchmark response (BMR) size (i.e. here, a 50% decrease in cell growth). Horizontal and vertical dashed lines represent this BMR of -50%, and the determination of the BMD-50, respectively, by interpolation from the fitted models. (**a**) On this basis, the "relative potency factor" (RPF) for the 16 nm-SiO_2 doses in RSCM compared to in NSCM can be determined. Here, this shows the *same* molar dose of 16 nm-SiO_2 is approximately ~2.4 times more potent in RSCM when compared to equivalent exposures in NSCM. In turn, the RPFL / RPFU, and BMDL / BMDU values represent the lower (L) and upper (U) bounds of each RPF or BMD value's two-sided, 90% confidence interval.

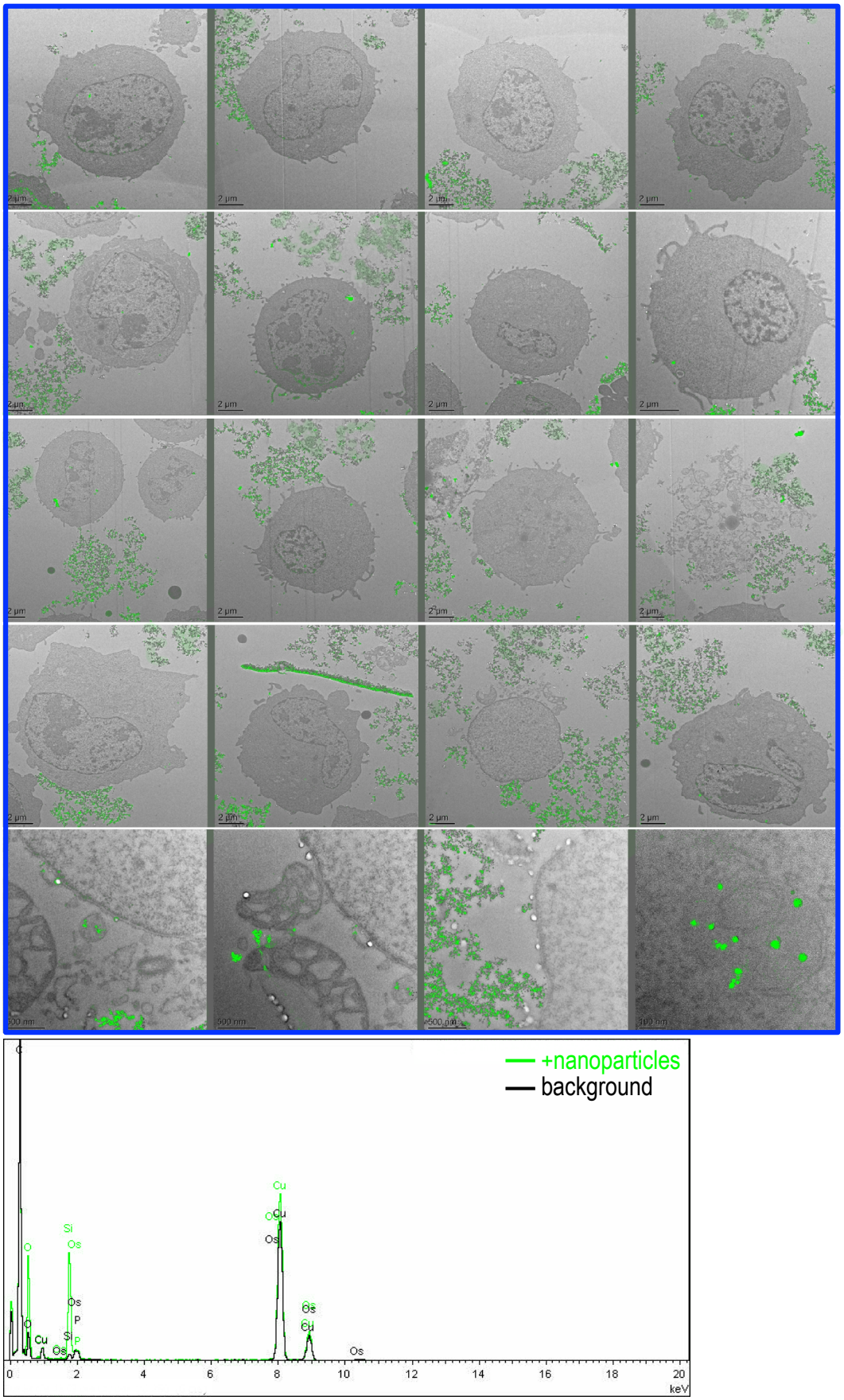

Figure S10 – Cellular delivery and uptake of 16 nm-SiO_2 in normal serum containing media (NSCM). Brightfield transmission electron micrographs obtained after 24 h exposure (73 nM dose). Efforts were made to image > 50 cell sections. Far fewer particles (false coloured green) were found surrounding the cell membranes and internalised within vesicles when compared to 16 nm-SiO_2 exposures in reduced serum containing media (RSCM) (see Figure S11). Nanoparticles were identified on the basis of their composition by energy dispersive x-ray (EDX) spectroscopy (example spectra shown, bottom). Background spectra (black) were overlaid with those from areas containing nanoparticles with the shift in the abundance of silicon and oxygen used to identify the particles (green). Copper and Osmium signals arose from the sample grids and staining employed to increase contrast, respectively.

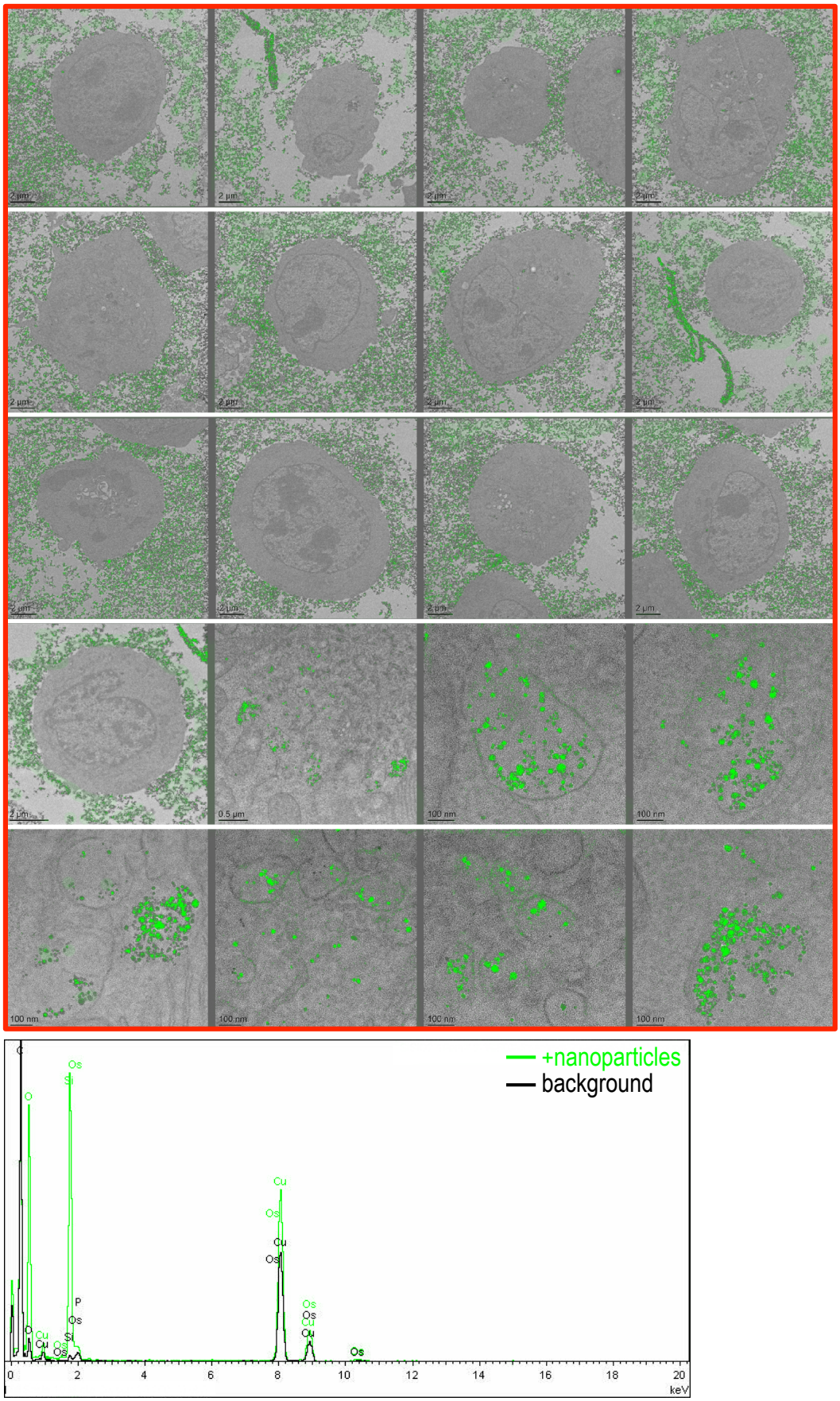

Figure S11 – Cellular delivery and uptake of 16 nm-SiO_2 in reduced serum containing media (RSCM). Brightfield transmission electron micrographs obtained after 24 h exposure (73 nM dose). Efforts were made to image > 50 cell sections. Much greater abundances of particles (false coloured green) were found surrounding the cell membranes and internalised within vesicles when compared to 16 nm-SiO_2 exposures in normal serum containing media (NSCM) (see Figure S10). Nanoparticles were identified on the basis of their composition by energy dispersive X-ray (EDX) spectroscopy (example spectra shown, bottom). Background spectra (black) were overlaid with those from areas containing nanoparticles with the shift in the abundance of silicon and oxygen used to identify the particles (green). Copper and Osmium signals arose from the sample grids and staining employed to increase contrast, respectively.

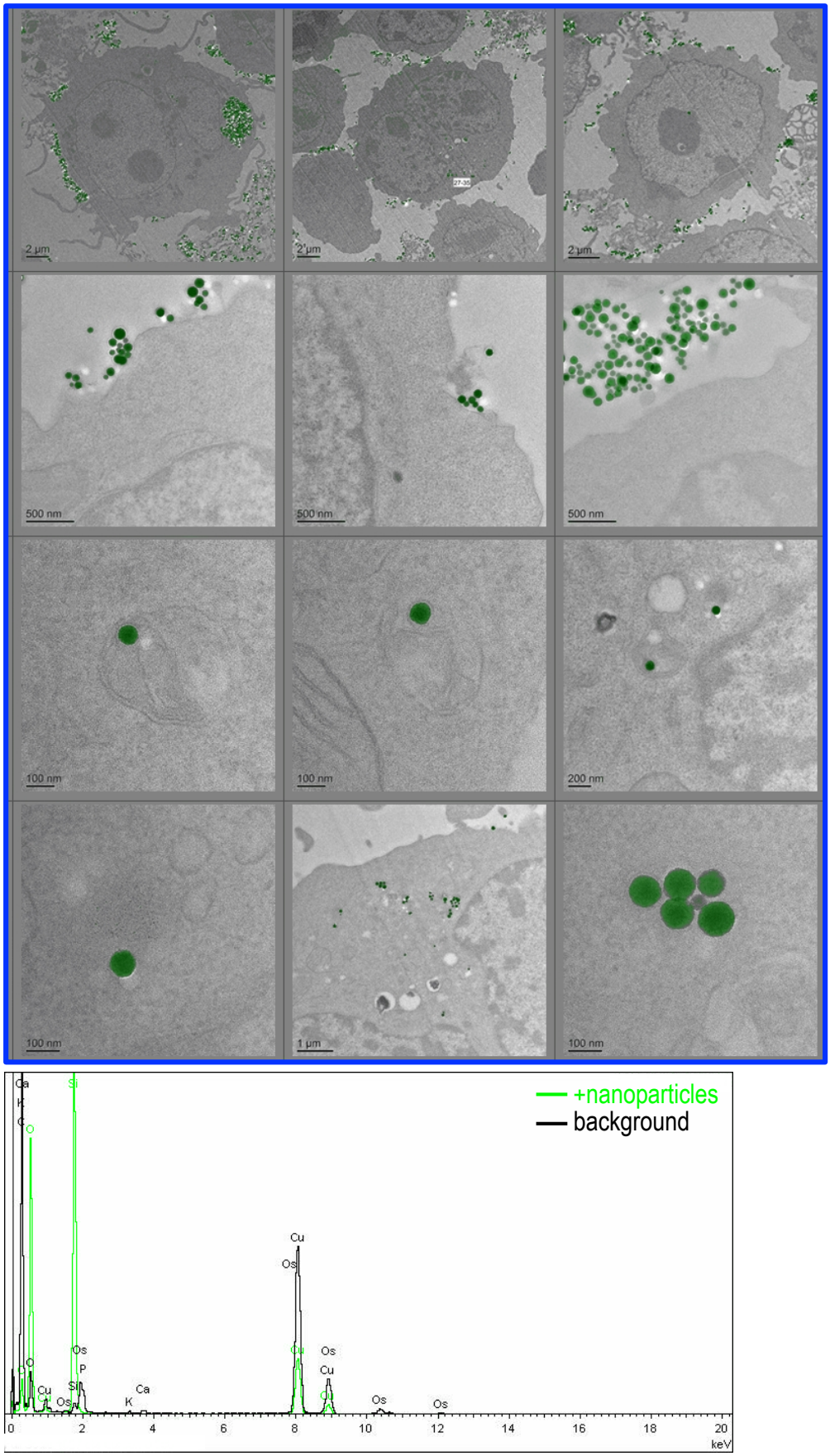

Figure S12 – Cellular delivery and uptake of 85 nm-SiO_2 in normal serum containing media (NSCM). Brightfield transmission electron micrographs obtained after 24 h exposure (0.5 nM dose). Efforts were made to image > 50 cell sections. In contrast to the 16 nm-SiO_2 findings, the abundances of 85 nm-SiO_2 particles (false coloured green) found surrounding the cell membranes and internalised within vesicles were similar regardless of serum environment. Nanoparticles were identified on the basis of their composition by energy dispersive X-ray (EDX) spectroscopy (example spectra shown, bottom). Background spectra (black) were overlaid with those from areas containing nanoparticles with the shift in the abundance of silicon and oxygen used to identify the particles (green). Copper and Osmium signals arose from the sample grids and staining employed to increase contrast, respectively.

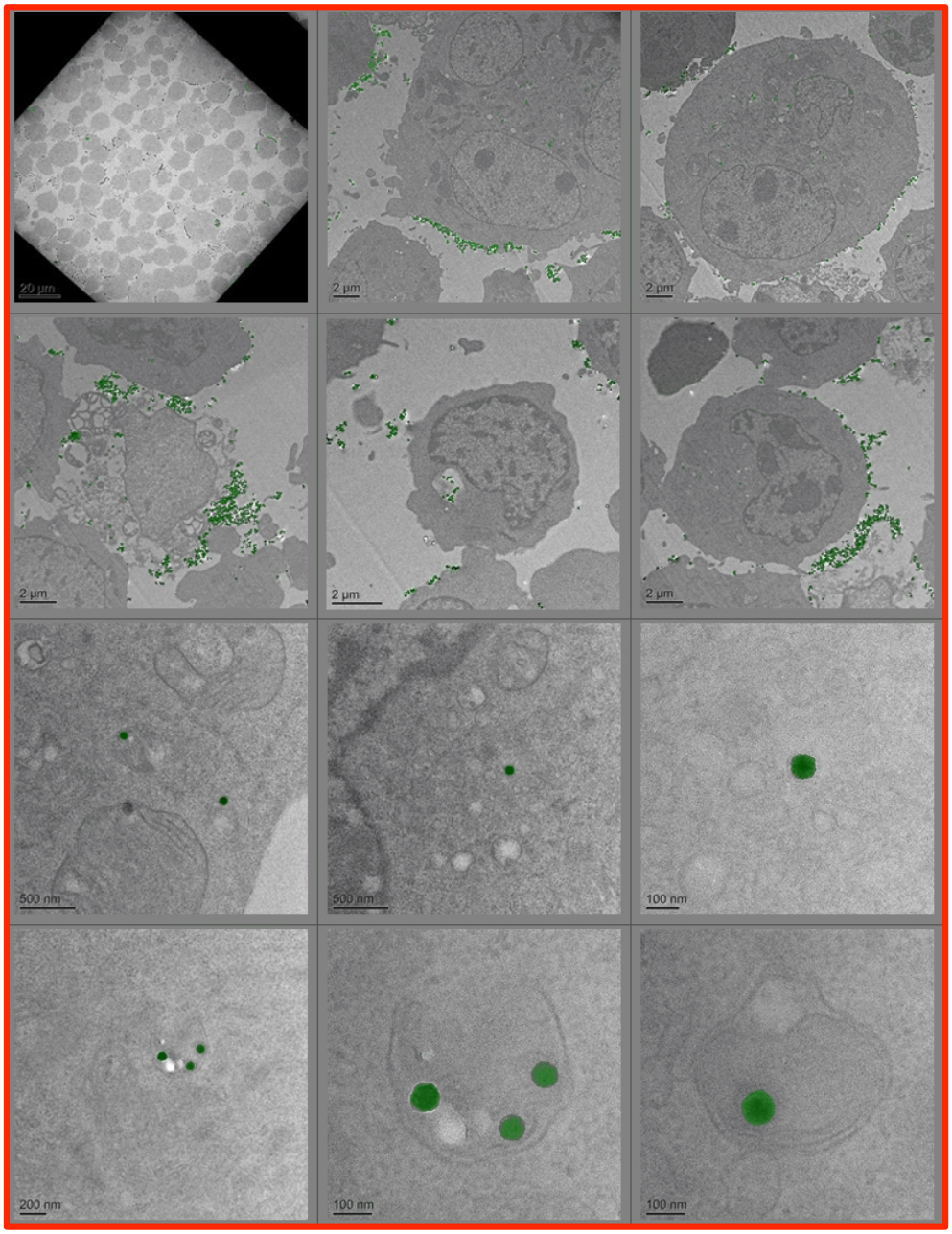

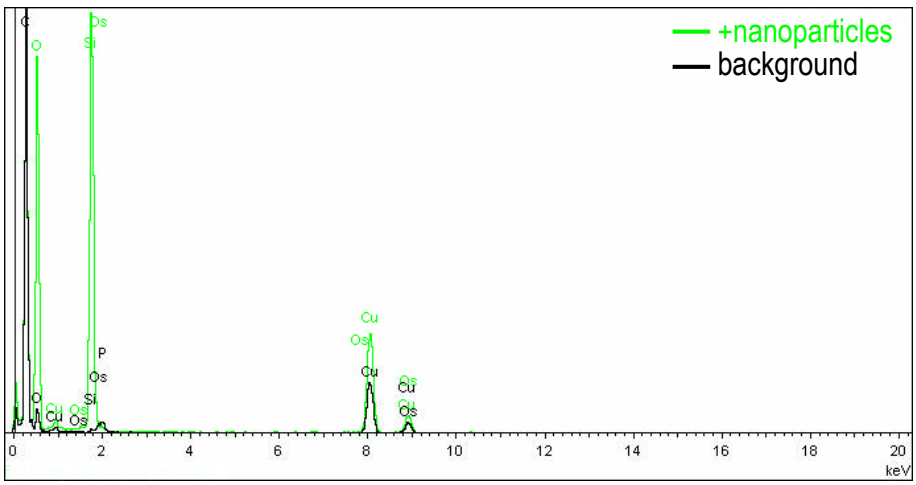

Figure S13 – Cellular delivery and uptake of 85 nm-SiO_2 in reduced serum containing media (RSCM). Brightfield transmission electron micrographs obtained after 24 h exposure (0.5 nM dose). Efforts were made to image > 50 cell sections. In contrast to the 16 nm-SiO_2 findings, the abundances of 85 nm-SiO_2 particles (false coloured green) found surrounding the cell membranes and internalised within vesicles were similar regardless of serum environment. Nanoparticles were identified on the basis of their composition by energy dispersive X-ray (EDX) spectroscopy (example spectra shown, bottom). Background spectra (black) were overlaid with those from areas containing nanoparticles with the shift in the abundance of silicon and oxygen used to identify the particles (green). Copper and Osmium signals arose from the sample grids and staining employed to increase contrast, respectively.

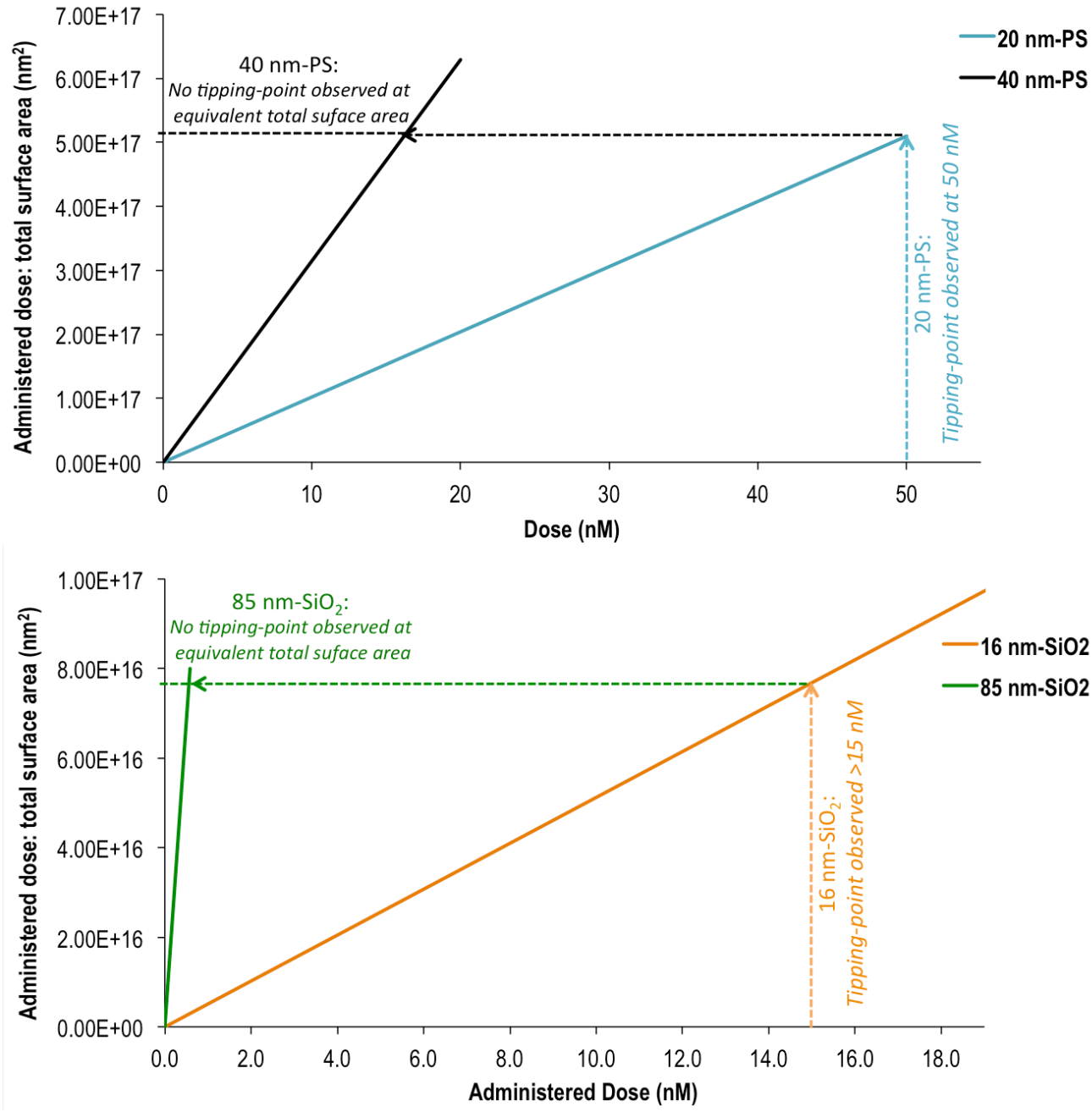

Figure S14 - Relationship between the administered nanoparticle dose, its total surface area and the occurrence of tipping-points in agglomeration state. Neither the 40 nm-PS or the 85nm-SiO_2 exposures elicited a tipping point in agglomeration state, despite utilisation of administered doses with equal or greater total surface areas (indicated, horizontal dashed lines) to those where the effect *was* observed (indicated, vertical dashed lines) for their smaller, yet otherwise identical counterparts (i.e. the 20 nm-PS and 16 nm-SiO_2). This shows that these tipping point events are not underpinned by a simple-to-predict, total surface area to serum relationship; necessitating robust agglomeration state characterisation techniques to permit their detection empirically.